The dynamics of plate boundaries over a convecting mantle

Laurent Husson

The dynamics of plate boundaries over a convecting mantle

Laurent Husson[a,b,*]

[a]*Géosciences Rennes, CNRS UMR 6118, Université de Rennes-1, France*
[b]*LPG Nantes, CNRS UMR 6112, Université de Nantes, France*

Abstract

Trench motion and upper plate deformation ultimately respond to mantle flow. In order to explore the dynamic relationship between the two aspects, I build upon the mantle flow model results of Conrad and Behn (2010) and compute the drag force underneath each plate. The small misfit angle between between the traction azimuths of mantle traction and absolute plate motion corroborates the idea that convective mantle drag is a prominent driver of plate tectonics. Less intuitive is the fact that the interplay between the drag forces from the upper and lower plates, that amounts to -5 to 8.5×10^{12} N m^{-1} (per unit trench length), dictates both trench migration rates and upper plate deformation. At odds with the classic view that assigns the prime role to local variations of slab pull, I find that variations in the intrinsic properties of subduction zones only modulate this behavior. More specifically, the mean value of the integrated trenchward mantle drag force from the lower and upper plates (from -2 to 6.5×10^{12} N m^{-1}) controls upper plate deformation. Conversely, it is the difference between the lower and upper plates mantle drag forces (from -3 to 10×10^{12} N m^{-1}) that controls trench migration rates. In addition, I find that a minimum trenchward force of approximately $2 - 2.5 \times 10^{12}$ N m^{-1} must be supplied by mantle drag before trenches can actually advance, and before upper plates undergo compression. This force results from the default tendency of slabs to rollback when solely excited by their own buoyancy, and is thus the effective tensional force that slab pull exerts on the plate interface.

Key words:

trench migration, orogenesis, interplate forces, subduction, mantle flow

1. Introduction: plate boundaries in a finite Earth

A glance at a physical map of the world shows that plate boundaries vary greatly from one another. Attempts to comprehensively classify them started more than 30 years ago (e.g., Chase, 1978; Uyeda and Kanamori, 1979; Ruff and Kanamori, 1980). However, the persistent literature on the dynamics of plate boundaries reveals that it remains a vivid, somewhat unresolved issue. Even the processes that operate at

plate boundaries are controversial and range from local to global scale interactions, or a combination of the two (e.g. Stadler et al., 2010).

The deformation of upper plates, as well as the surface migration of the trench (Fig. 1) are the prevailing observables of interplate dynamics, and substantial work has taken advantage of these quantifiable features (e.g., Ruff and Kanamori, 1980; Jarrard, 1986; Garfunkel et al., 1986; Heuret and Lallemand, 2005; Lallemand et al., 2005, 2008; Funiciello et al., 2008; Schellart, 2008). On this basis, the usual way to classify plate boundaries is to cross-correlate the kinematical and geometrical properties of plate boundaries, that should ultimately mirror their dynamics. Ruff and Kanamori (1980) suggested that back-arc deformation responds to the coupling between the upper and lower plates, that coupling itself relating to the slab age-buoyancy. Uyeda and Kanamori (1979), or more recently Heuret and Lallemand (2005), instead found that back-arc deformation roughly correlate with upper plate velocity. As to trench migration rates, Lallemand et al. (2008) found that they are chiefly controlled by lower plate velocity, which in turns depends on the slab age buoyancy. But the authors also indicate that the relationship breaks down where upper plates are deforming, and suggest that many subduction zones depart from a kinematic equilibrium that is required for such analysis. In addition, they also found (Heuret and Lallemand, 2005) that many subduction zones depart from theoretical rules: global statistics show that observations depart from theory by 180 degrees when comparing trench migration and, for instance, the thermal age and pull of slabs. Indeed, while theory suggests that trenches should retreat faster for old slabs, observations show the opposite tendency. Departure from the intuitive behavior laws were further explored by invoking the many local -or intrinsic- parameters of subduction zones (see e.g., Billen, 2008; Gerya, 2011, for reviews).

Another issue may reside in the fact that subduction zones on Earth are not that many. This may render statistical approaches misleading because subduction zones are not isolated systems. The local kinematics at a given subduction zone is in fact a blurred by-product of global dynamics. For instance, the Pacific subduction zones (more than two third of the current subduction zones on Earth) dynamically influence one another (e.g. Husson et al., 2008; Nagel et al., 2008; Gérault et al., 2012). Even at a larger scale, the Indo-Eurasian collision modified the kinematics of the Atlantic domain (Conrad and Lithgow-Bertelloni, 2007). Furthermore, recent case studies (Becker and Faccenna, 2011; Cande and Stegman, 2011; Husson et al., 2011) revealed that mantle drag is a primordial, yet seldom quantified, source of force that may help reconcile observations and theory. Thus in this paper, I explore the possibility that variations of the slab pull force -and more generally any intrinsic property of a given subduction zone- does not explain these discrepancies and that instead, global plate tectonics viewed in the framework of convection may explain interplate dynamics. I thus compute mantle traction forces and match the observed dynamics of subduction zones against mantle drag underneath converging plates.

2. Force balance at plate boundaries and interplate kinematics

In order to explore the dynamics of plate boundaries, I take advantage of the existing databases for trench migration and upper plate deformation (Lallemand et al., 2005; Heuret and Lallemand, 2005; Funiciello et al., 2008); I discarded ten data points from the original databases because they belong to slabs that are too small when compared to the resolution of the current study, and for which the local processes may prevail. I consider trench migration rates in the four representative reference frames chosen by Funiciello et al. (2008, Fig. 1): $SB04$ (Steinberger et al., 2004), $HS3$ (Gripp and Gordon, 2002), $GJ86$ (Gordon and Jurdy, 1986) and NNR (DeMets et al., 1994). Note that the last one, NNR is kinematically defined and by no means rooted on a dynamic ground. For upper plate deformation, I will use the UPS (Upper Plate Strain) qualitative parameter of Heuret and Lallemand (2005) that ranges from highly Compressive (C3) to highly Extensive (E3). In the following, I dropped the prefixes C and E and simply swapped E for a negative sign.

2.1. Kinematics at plate boundaries: trench migration and upper plate deformation

From a dynamic viewpoint, trench migration can be described as the result from the imbalance between the forces exerted by the lower and upper plates at the plate interface, F_{lp} and F_{up}, the missing term being viscous dissipation in the underlying mantle $VD = |F_{lp} - F_{up}|$. A schematic view, in two dimensions, would be that of the drift of the entire surface system including both the plates and the trench, accompanied by a laminar flow in the underlying mantle (Fig. 2). For a Newtonian rheology, trench velocity should therefore scale with $F_{lp} - F_{up}$ (both F_{lp} and F_{up} being counted positive trenchward). This behavior is exemplified by the Pacific system that possibly drifts to the West as a response to the westward force at the plate boundary (Husson et al., 2008). The force exerted by the South American plate exceeds the resistance of the lower plate, and is accommodated by the viscous shear of the Pacific mantle.

Mountain building, or more generally upper plate deformation, conversely results from the mean force that is exerted at their boundaries, _i.e._ F_{lp} and F_{up}, such that the orogenic load $OL = (F_{lp} + F_{up})/2$, where F_{lp} and F_{up} being counted positive trenchward (Fig. 2). Note that the orogenic load equals the sum of the buoyancy and viscous forces in the lithosphere, in the deforming plate boundary (e.g., England and McKenzie, 1982; Husson and Ricard, 2004). If both plates are pushing towards the trench, compression at the plate interface is expected, as well as mountain building, and conversely, back-arc extension will typically arise if the net force is extensive. In a comparable way to trench migration, upper plate deformation should therefore scale with $\Sigma_F = (F_{lp} + F_{up})/2$.

3

If correct, and as obvious as it may sound, there should be a correlation between the force balance at the plate boundaries and the dynamics of the plate margin. However, and this is less obvious, because trench migration and upper plate deformation depend on the same forces, they may also correlate to one another *via* the quantities F_{lp} and F_{up}. Those forces result from sources that are distributed over the entire plates, and not restricted to the subduction zones *sensu-stricto*. Heuret and Lallemand (2005) concluded that upper plate strain and trench migration are poorly correlated. Indeed, no regression by a monotonic function gives a satisfying fit. However, further exploration yields different conclusions, particularly when considering multiple reference frames, and above all when considering circum-Pacific trenches only (Fig. 3). Interestingly, the relationship is not linear but there rather seems to be a threshold at $UPS \sim -1$: Figure 3 reveals a bimodal distribution for trench migration rates V_t, particularly for the Pacific domain. Some 70% circum-Pacific trenches are jointly retreating and compressive to moderately extensive, while some 25% are jointly advancing and strongly extensive: together, it indicates that some 95% of the trenches corroborate the existence of a relationship that ties UPS to V_t. In the three dynamically-based reference frames ($SB04$ (Steinberger et al., 2004), $HS3$ (Gripp and Gordon, 2002), $GJ86$ (Gordon and Jurdy, 1986)), retreating trenches are associated to compression and reciprocally, advancing trenches are associated to extension (Fig. 3). Note that because NNR is not a dynamically consistent reference frame, it is no surprise that this relationship breaks down. The few outliers (less than 5% of the dataset) correspond to the Lau and Yap trenches. Their behavior departs from the general behavior of the Pacific domain, most likely because of their atypical location at slab edges, allowing for idiosyncratic mantle flow to develop. Non-Pacific sites chiefly correspond to the Java-Sumatra, Philippines, and Caribbean subduction zones; they mostly depart from the correlation between UPS and V_t. This may be interpreted by the fact that they all lay close to the Pacific system, that not only overwhelms the statistics, but also the dynamics of mantle flow at the global scale (see section 4.1).

2.2. Computing the forces at play at the plate interface, F_{lp} and F_{up}

The driving force exerted by the upper plate F_{up} onto the plate interface (Fig. 2) results from the drag from the underlying flowing mantle md_{up}, and from a far-field contribution rp_{up} that corresponds to the ridge push on the upper plate side (that should in principle be modulated by plate interactions at the other boundaries of the upper plates, see discussion), and writes $F_{up} = md_{up} + rp_{up}$. On the lower plate side, the force F_{lp} that applies on the trench similarly writes $F_{lp} = md_{lp} + sp^{\star} + rp_{lp}$, where rp_{lp} and $sp^{\star}$ respectively denote the ridge push (similarly to rp_{up}) and the effective contribution of slab pull (*i.e.* the force exerted by the mass anomaly of the slab minus the viscous dissipation in both the bending slab and surrounding mantle). Ridge push varies like the thermal age of the subducting slab (e.g Parsons and Richter, 1980; Turcotte and Schubert, 1982), which is most likely capped at 80 Ma (Carlson and Johnson, 1994). This

leaves a maximum value of $\approx 3 \times 10^{12}$ N m^{-1}, *i.e.* relatively small compared to the driving forces of plate tectonics (e.g. Turcotte and Schubert, 1982).

Global mantle flow models yield quantitative estimates of basal drag md. In order to evaluate its contribution globally, I take advantage of the model results from Conrad and Behn (2010), that provide the shear traction field underneath the lithosphere, which uses the finite element model CitcomS (Zhong et al., 2000; Tan et al., 2006). The model is density-driven, wherein mantle flow is excited by mantle density heterogeneities as inferred from seismic tomography (S20RTSb, Ritsema et al., 2004). The seismic velocity structure below 300 km converts into a density structure using a conversion factor that is here set to 0.17 g cm^{-3} km^{-1} s (in adequation to the recent results of Husson et al. (2011), comparable to the earlier models of Conrad and Behn (2010), after Karato and Karki (2001)). This conversion is done under the arguable assumption that all anomalies are thermal, as opposed to chemical, in origin. Within the shallowest 300 km, density anomalies are set to null because the straightforward conversion from seismic tomography to density notoriously breaks down at those depths. This model is instantaneous and buoyancy-driven. Surface conditions are no slip, free slip is imposed at the core-mantle boundary. The lower mantle has a uniform viscosity (below 670 km), an asthenosphere (above 300 km and below the lithospheric base), and a lithosphere, with reference viscosities that are 50, 0.1, and up to 1000 times the reference viscosity of the upper mantle (300 to 670 km). Low-viscosity asthenosphere smoothly transitions into high viscosity lithosphere, which has a variable thickness that is consistent with seafloor age (for oceans) or near-surface tomography (for continents). These models give predictions of the driving component of the shear traction field beneath the lithosphere. In practice, the force that arises from the slab load is partially transmitted to the unsubducted part of the lithosphere *via* the viscosity structure, the remainder being either transmitted to the lithosphere as mantle drag or diffused in the deforming mantle. Therefore, the rheological structure of the model implies that slab pull is implicitly accounted for (below 300 km depth). Interplate forces thus reduce to

$$F_{up} = md_{up} + rp_{up}, \tag{1}$$

$$F_{lp} = md_{lp}^{\star} + rp_{lp}, \tag{2}$$

where $md_{lp}^{\star} = md_{lp} + sp^{\star}$. Upon the model approximations, basal drag is thus most likely the major contributor, that I examine in the following.

To estimate the net drag force that drives each plate, I expand on previous work (Husson et al., 2011) wherein we computed the net drag force for the South American plate. I first compute the total torque T_s exerted by the internally driven shear tractions beneath each individual plate. This simply writes $T_s = \int_s \mathbf{r} \times \tau ds$, where $\mathbf{r}$ is the radial unit vector, τ is the local shear stress, and s is the area of the plate.

5

This yields Euler poles for each individual plate, around which small circles show the principal direction of traction underneath (Fig. 4b). I then project the local net shear traction vectors within each plate along the small circles that circumscribe the Euler poles and integrate them along each portion of small circles, from one end to the other across the plates. This yields a force per unit length, out of which I extract the normal component to the trench, that is represented on Fig. 4b along both sides of each plate boundary (note that the value at an end of a given small circle is the opposite of its other end counterpart).

3. Results

3.1. Mantle drag and absolute plate motion

Mantle drag drives plate and should be consistent with plate motion (e.g., Becker and O'Connell, 2001; Van Summeren et al., 2012). The computed Euler poles indeed reveal that mantle tractions are remarkably consistent with plate motion: plates are driven away from ridges and converge towards subduction zones, and small circles mostly intersect trenches at a high angle, almost normal. More specifically, the Pacific and South American plates are driven to the West, the African, Arabian, Indian, and Australian plates are pushed towards Eurasia, and the Nazca plate towards South America. Even the smaller Philippines and Arabian plates are conformably converging towards their overriding plates. Antarctica, which is entirely surrounded by ridges, is essentially stationary for its Euler pole lie within the plate itself. The angular distance between the dynamic (predicted) and kinematic (observed) Euler poles can be used as a metric to quantify the quality of the fit between the computed torques and observed plate motion. For all plates including the smallest considered (Juan de Fuca), and in any reference frame, it is always smaller than $90°$ (full misfit would be $180°$), implying that the match is never negative. The mean distance is $\sim 45°$ in all reference frames, which indicates that the misfit between the mean traction azimuth from mantle flow and absolute plate motion is $\sim 22.5°$. The misfit decreases when small plates (Juan de Fuca, Scotia, Cocos, Caribbean, and Arabian plates) are discarded, revealing the resolution limit of the model. In addition, the fit between dynamic and kinematic poles significantly improves for fast moving plates ($\sim 27°$ on average for the Pacific, Australian, Philippines, Nazca and South American plates, in dynamic reference frames). For those plates, the misfit between the mean traction azimuth from mantle flow and absolute plate motion is only $\sim 15°$. Overall, this good fit shows that the mantle drag component is at least compatible with plate motion, and most likely reveals that it is the principal contributor. This model, however, includes a rheological structure that makes both *suction* and *slab pull* (Conrad and Lithgow-Bertelloni, 2002, 2004) indeterminately embedded in the model. As such, some of the drag force here is the same force as the slab pull force in these comparable studies, that yield similar results. Last, this result suggests that this quantification of interplate tractions from Conrad and Behn (2010) is valid and may be used to infer how

mantle drag may control the dynamics of plate boundaries.

Some systematics can be inferred at convergent plate boundaries from the integrated drag forces shown Fig. 4b. The forces are essentially negative along ridges and positive along convergent zones, respectively favoring kinematic divergence and convergence conformably to surface tectonics. To summarize, lower plates are systematically dragged toward the subduction zones, both upper and lower plates are dragged toward the trench where the Alps, Himalayas, and Andes are, and upper plates are dragged away from the subduction zone where back-arc basins are found, for instance the Philippine plate at the Mariana trench and the Australian plate at the Tonga-Kermadec trench.

More can be said from a quantitative analysis. Trench migration and upper plate deformation should scale with $(F_{lp} - F_{up})$ and $(F_{lp} + F_{up})/2$, respectively (see section 2.1). The good fit between mantle drag and plate motion implies that mantle drag systematically adds up to ridge push in a complementary fashion, mutually reinforcing one another. In addition, because the mean absolute value of the integrated traction is $3.7 \times 10^{12} \ N \ m^{-1}$ (standard deviation is $2.4 \times 10^{12} \ N \ m^{-1}$), its impact on the force balance is thus at least comparable and often higher than the ridge push. Thus, it comes from the expressions (1) and (2) that F_{up} and F_{lp} may be dominated by their basal drag force md_{up} and md_{lp} that are examined herein.

3.2. Mantle drag and trench migration rates

Figure 5a shows the difference between the trenchward integrated drag force $\Delta md = md_{lp} - md_{up}$, together with the normal component of trench migration in the reference frame $SB04$ (this reference frame has a net rotation component that is intermediate between NNR and $HS3$). Trench motion is essentially normal to the trench (fig. 1) so it is a good parameter to comp rare the force balance with. Some 88% of the Δmd values are positive, which means that the mantle generally drags the lower plate towards the trench more vigorously than the upper plate. The remaining 12% negative values are all retreating regardless of the reference frame (besides NNR, Fig. 6). Contrarily, all advancing trenches have positive values for Δmd (Fig. 6). This result can be explained by the fact that negative values of Δmd correspond to trenches where the force balance reinforce the natural tendency of trenches to retreat as a response to slab buoyancy (Kincaid and Olson, 1987; Funiciello et al., 2003; Bellahsen et al., 2005; Stegman et al., 2006; Royden and Husson, 2006; Capitanio et al., 2007; Di Giuseppe et al., 2009; Goes et al., 2011), therefore rendering trench retreat the unique admissible mode. Furthermore, it indicates that trenches can advance only if the trenchward drag force from the lower plate overwhelms that tendency.

Overall, there is a loose negative correlation of trench migration rates with Δmd. That correlation is reinforced when only circum-Pacific trenches are considered (Fig. 6). Note that I excluded Alaska and Aleutian trenches, because the drag force is above all tangential to the trench (both in North America and Pacific), and although compatible with the general results, the model likely breaks down for such low angles between the forces and trench directions (Fig. 4b). For other circum-Pacific trenches, a bimodal distribution prevails, with a threshold at $\sim 2 \times 10^{12}$ N m^{-1} that is valid in all considered reference frames but NNR (Fig. 7). The fact that the optimal threshold is not at 0 N m^{-1} indicates that Δmd must overcome some minimal force before trenches can advance. Thus, 2×10^{12} N m^{-1} may be interpreted as the average force that the intrinsic properties of subduction zones (mostly slab buoyancy) exert on trenches to make them retreat by default.

Interestingly, the relationship between Δmd and trench migration rates V_t also holds at a lower scale, *i.e.* within a unique subduction zone. For instance along the Tonga-Kermadec subduction zone, the trench retreats extremely fast along its northern part, where Δmd reaches the most negative value. Trench retreat rates decrease southward and the trench eventually advances along the Kermadec section, where Δmd becomes positive (Fig. 5a). Similar observations can be made along the Nazca subduction zone, where trenches retreat faster along the Columbia and Peruvian trenches, where Δmd is negative, than along the Chile trench where Δmd is positive.

3.3. Strain rate and mountain building in plate boundary zones

Figure 5b shows the mean of the trenchward integrated drag forces $\Sigma md/2 = (md_{lp} + md_{up})/2$, together with the qualitative estimates of upper plate strain UPS from Heuret and Lallemand (2005). Obviously, maximum compression is found where mountain belts are, in the Andes (up to 5×10^{12} N m^{-1}), and maximum extension is predicted for the Tonga trench, that bounds the very fast opening Lau basin. Some 77% of the values are positive, indicating that the drag forces from the lower and upper plates are mostly converging. The remaining 23% are essentially showing extension, besides Alaska that shows a moderate compression ($UPS = 0$ to 1), but that should be set aside (see above). Almost all trenches that display positive values for UPS also display positive values for Σmd, indicating that compression can only be achieved where the drag forces from upper and lower plates are converging, while the reciprocal is not true: extension can occur even when the drag forces are converging. This can also be explained by the role of the intrinsic properties of subduction zones. The most natural mode of subduction is rollback, which induces extension on the overriding plate, and that extensional force needs to be overcome before compression can occur.

A trend exists between UPS and $\Sigma md/2$ (Fig. 8), that is re-enforced when circum-Pacific data are selected (and the Alsakan and Aleutian subduction zones are dismissed). Again, it is more a bimodal distribution that prevails than a continuous function (Fig. 9). 91% have positive UPS values for $\Sigma md >$

$2.5 \times 10^{12}~N~m^{-1}$, while 85% have negative or neutral UPS values when $\Sigma md < 2.5 \times 10^{12}~N~m^{-1}$. Again, the optimal threshold is not null: Σmd must overcome a minimal value before compression can surely occur. I interpret this threshold as the magnitude of the force that is exerted onto the plate interface, on average, by the natural tendency of slabs to rollback as a response to their own buoyancy.

Again, the inferred relationship holds at lower scales. Figure 10 shows the latitudinal dependency of UPS and of the drag force for East Pacific trenches, together with the buoyancy forces from the adjacent mountain belts. Along the Nazca trench, maximum compression is found where the cumulated drag force is maximal. Both compression and UPS decrease from the Central Andes to the northern and southern ends of the Andean belt. Interestingly, it also compares to the buoyancy forces (or gravitational potential energy) due to the load of the mountain belt itself (fig. 10, see also Husson et al., 2011). The maximum buoyancy force, in the Central Andes, amounts to almost $10~10^{12}~N~m^{-1}$ and decreases towards the ends of the mountain belts by more than $7~10^{12}~N~m^{-1}$. The mean drag force shows a similar signal, though shifted to lower magnitudes by $\sim 2.5~10^{12}~N~m^{-1}$. That constant could be seen as an even contribution from ridge push, here unaccounted for. Of course, crustal thickening is an indicator of upper plate deformation, and thus directly relates to UPS. This additional fit reinforces the hypothesis that mantle drag is responsible for interplate dynamics, as characterized by upper plate deformation (mountain building and strain rates), as well as trench migration rates. Similalry, latitudinal correlation is found in the Southwest Pacific, where the mean cumulated drag force decreases from the Kermadec trench to the Tonga trench by $\sim 2 \times 10^{12}~N~m^{-1}$, while deformation evolves from minor compression to strong extension (see fig. 5).

4. Discussion

4.1. Far field forces vs effective slab pull force

The threshold forces that are found for the bimodal distributions of V_t and UPS amount to $2 \times 10^{12}~N~m^{-1}$ to $2.5 \times 10^{12}~N~m^{-1}$, respectively. In both cases, I interpret this threshold as the tensional force due to the default tendency of slabs to rollback. Therefore, I suggest that this value is an indirect estimate of the tensional component induced by the intrinsic properties of subduction zones, *i.e.* the balance between the slab pull force and the viscous dissipation in the bending slab and surrounding mantle. This metric, that could be referred to as the *effective slab pull force* should then be anchored to the kinematic relationship of Lallemand et al. (2008), $V_t = 0.5 V_{sub} - 2.3~cm/yr$, where V_{sub} is the subducting plate velocity, that applies to trenches that are considered stress free. Upon that stress condition, upper plates passively accompany trenches, and prevent upper plates from modifying the subduction dynamics (Yamato et al., 2009; Capitanio et al., 2010). That condition is given from a kinematic standpoint of Lallemand et al. by $UPS = 0$, and from the dynamic standpoint of the current study by a trenchward mantle drag force underneath the lower

plate md_{lp} that exceeds that from the upper plate md_{up} by ~ 2 or 2.5×10^{12} N m^{-1}.

4.2. Exploiting the Pacific bias

The fact that a bimodal distribution prevails as regards the interplate drag forces for both V_t and UPS is intriguing. The above explanation does not give any insight on a functional discontinuity. Instead, it results from a sampling bias due to the fact that subduction zones are in limited numbers and that the Pacific subduction system dominates the signal. Its Western and Eastern margins notoriously feature self consistent geometric and kinematic properties, coined as the Chile and Mariana types of Uyeda and Kanamori (1979). The two groups from the Pacific overwhelm the statistic, which explains the bimodal rather than continuous distribution. In addition, the current results seemingly exclude a few outliers, but these breakdowns in the inferred relationships may in fact help to unravel mantle dynamics. For instance, a few trenches (chiefly Java-Sumatra, Philippines and Caribbean) are advancing while Δmd is only moderately positive ($\sim 2 \times 10^{12}$ N m^{-1}, Fig. 6). These subduction zones lay on the outer margin of the Pacific domain. This may indicate that those trenches are being pulled by the nearby Pacific trenches, whose size is much larger. Technically, it implies that the underlying hypothesis -that plates are chiefly driven by mantle drag underneath them only- may become invalid. Plates interact with each other, *i.e.* stresses are continuous and thus transmitted across their boundaries. Trench velocities for the Java-Sumatra and Philippines subduction zones converge towards the Eastern Pacific subduction zones (Fig. 1), which may illustrate that process. Similar reasoning may hold for the Caribbean subduction zone, whose trench is counter-intuitively dragged towards the Western Pacific zone.

4.3. Viscosity of the lithosphere and upper mantle

The soundness of the results can be tested *via* back-of-the-envelope calculations that predict orders of magnitudes for the viscosity. First, the simple, two-dimensional view of trench migration (Fig. 2) simply yields, on average

$$\frac{\overline{F_{lp} - F_{up}}}{\overline{W}} = \eta_m \frac{\partial v}{\partial z}, \tag{3}$$

where $\overline{V_t}$, $\overline{W}$, η_m and $\frac{\partial v}{\partial z}$ are the mean trench velocity, the characteristic width of the sheared system, the viscosity of the upper mantle, and the horizontal velocity gradient in the vertical direction. In the above Couette flow approximation, $\overline{\Delta_F}$ and $\overline{V_t}$ scale with η_m:

$$\eta_m = \frac{|\overline{\Delta F}|}{\overline{W}} \frac{h}{|\overline{V_t}|}, \tag{4}$$

where h is the thickness of the upper mantle. For circum-Pacific trenches, $|\overline{\Delta_F}| = 3.4 \times 10^{12} N$ m^{-1}, $|\overline{V_t}| = 16.5$ mm/yr (mean absolute value in the reference frame $SB04$), $h = 670$ km and $\overline{W} \simeq 10000$ km.

10

This yields $\eta_m \simeq 4 \ 10^{20} \ Pa \ s$, which is typically in the range of acceptable values for the viscosity of the upper mantle (e.g. Lambeck and Chappell, 2001; Steinberger et al., 2004; Mitrovica and Forte, 2004).

Similarly, the deformation of the upper plate scales with the lithospheric viscosity, with

$$\Sigma_F/2 = (F_{lp} + F_{up})/2 = L\eta_L\dot{\epsilon}, \tag{5}$$

where η_L and L are the viscosity and thickness of the overriding lithosphere. Unfortunately, we don't have direct access to a metric of the longterm strain rate $\dot{\epsilon}$, but to the qualitative evaluation UPS from Heuret and Lallemand (2005). Instead, the world strain map (Kreemer et al., 2003) provides us with an estimate of the current strain rates. Upon the crude assumption that it is statistically equivalent to the longterm strain rate, one can grossly estimate the strain rate at subduction zones on this basis. Fast deforming areas, such as the Andes or Lau basin, where $|UPS| = 3$, typically show $\dot{\epsilon} \simeq 10^{-14} \ s^{-1}$, while Σ_F increases by $7.5 \times 10^{12} \ N \ m^{-1}$ between $UPS = -3$ and $UPS = 3$ (from the crude regression of Fig. 8). This yields $d(\Sigma_F/2)/d\dot{\epsilon} \simeq 2 \ 10^{26} \ N \ s$. Therefore, setting $L = 100 \ km$, one gets $\eta_L \simeq 2 \ 10^{21} \ Pa \ s$ from equation (5), which is a plausible value for the effective viscosity of the deforming lithosphere at plate boundaries (e.g., Husson and Ricard, 2004). Of course, uncertainty is much too large (Fig. 8) to be conclusive, but this suggests that our results are at least not absurd.

4.4. Absolute plate speed

Mantle drag correlates with the azimuth of plate motion; in addition, it may in principle be expected to dictate the magnitude of absolute plate velocity. The correlation is poor (see Fig. S1, Supplementary data). This results from the efficient modulation of plate velocity by the orogenic load (Iaffaldano et al., 2006; Martinod et al., 2010; Iaffaldano et al., 2011), or coupling, that is not accounted for. In that sense, the orogenic load that I tentatively compare to $\Sigma md/2 = (md_{lp} + md_{up})2$ could scale with plate velocity. Again, the correlation between $\Sigma md/2$ and absolute plate motion is poor. This is due to the fact that md varies spatially, from one trench to another, and there is therefore no baseline to compare the results with. Instead, some normalized blend of the mantle drag force md and of the resistance at the plate boundary Σmd would possibly yield a better result, but may eventually convert this simple first order comparison into a full integration of all driving and resisting torques (as, for instance, in Becker and O'Connell, 2001) that is beyond the scope of this paper.

11

5. Conclusions

A side product of this work is the computation of the integrated mantle drag for each plate. It is noteworthy that this value yields excellent correlation between the azimuth of mantle drag and that of plate motion. On average, the misfit angle between the two is $\sim 22.5°$, *i.e.* 12.5%. Moreover, fast plates are better resolved than slow plates (the misfit reduces to $\sim 15°$, *i.e.* 8%, when only the Pacific, Australian, Philippines, Nazca and South American plates are accounted for). This corroborates the idea that mantle drag is the primordial driver of plate tectonics. Plate speed is not satisfactorily predicted because of the coupling at plate boundaries, that modulates the velocity, but not the direction of plate motion.

Many studies (e.g. Ruff and Kanamori, 1980; Lallemand et al., 2008) relate trench kinematics to slab pull, and upper plate strain to upper plate motion. The dynamic relationship that is presented here encompasses the active contributions of both the upper and lower plates, and conversely explains contrasted modes of upper plate deformation. Mountain building are found above subduction zones provided that both plates are actively dragged against each other by the underlying mantle. Conversely, extension may occur if at least the upper plate is driven away from the trench by the flowing mantle. Thus, the current results assign a prime role to mantle drag and suggest that local idiosyncrasies of subduction zones only modulate interplate dynamics. More generally, intrinsic properties of subduction zones, for example water content, lubrification or local rheologies, only make observation depart from the behavior laws relating V_t to Δmd and UPS to $\Sigma md/2$, to a lesser extent than mantle traction does.

In the current paradigm, plates are not isolated from the convecting mantle and thus subduction zones are not anything different from a component of mantle convection. The vertical descent of slabs drives plates, as any other density anomaly whose force is transmitted *via* the rheological structure of the mantle. The force that slab pull effectively exerts at the plate boundary can in turn be indirectly quantified by the minimum excess force from md_{lp} with respect to md_{up} that is required before trenches can advance. Below this threshold, trenches will retreat and upper plates will undergo extension. That threshold amounts to $\sim 2.5 \times 10^{12} \ N \ m^{-1}$ and corresponds to the suction force that is exerted by the intrinsic properties of the subduction zone, slab pull in particular.

12

References

Becker, T. W., Faccenna, C., Oct. 2011. Mantle conveyor beneath the Tethyan collisional belt. Earth and Planetary Science Letters 310, 453–461.

Becker, T. W., O'Connell, R. J., 2001. Predicting plate velocities with geodynamic models. Geochemistry, Geophysics, Geosystems 2 (12).

Bellahsen, N., Faccenna, C., Funiciello, F., Jan. 2005. Dynamics of subduction and plate motion in laboratory experiments: Insights into the "plate tectonics" behavior of the Earth. Journal of Geophysical Research 110, 1401.

Billen, M. I., May 2008. Modeling the Dynamics of Subducting Slabs. Annual Review of Earth and Planetary Sciences 36, 325–356.

Cande, S. C., Stegman, D. R., Jul. 2011. Indian and African plate motions driven by the push force of the Réunion plume head. Nature 475, 47–52.

Capitanio, F. A., Morra, G., Goes, S., Oct. 2007. Dynamic models of downgoing plate-buoyancy driven subduction: Subduction motions and energy dissipation. Earth and Planetary Science Letters 262, 284–297.

Capitanio, F. A., Stegman, D. R., Moresi, L. N., Sharples, W., Mar. 2010. Upper plate controls on deep subduction, trench migrations and deformations at convergent margins. Tectonophysics 483, 80–92.

Carlson, R. L., Johnson, H. P., Feb. 1994. On modeling the thermal evolution of the oceanic upper mantle: An assessment of the cooling plate model. Journal of Geophysical Research 99, 3201–3214.

Chase, C. G., Nov. 1978. Extension behind island arcs and motions relative to hot spots. Journal of Geophysical Research 83, 5385–5388.

Conrad, C. P., Behn, M. D., May 2010. Constraints on lithosphere net rotation and asthenospheric viscosity from global mantle flow models and seismic anisotropy. Geochemistry, Geophysics, Geosystems 110, 5.

Conrad, C. P., Lithgow-Bertelloni, C., Oct. 2002. How Mantle Slabs Drive Plate Tectonics. Science 298, 207–210.

Conrad, C. P., Lithgow-Bertelloni, C., Oct. 2004. The temporal evolution of plate driving forces: Importance of "slab suction" versus "slab pull" during the Cenozoic. Journal of Geophysical Research (Solid Earth) 109, 10407.

Conrad, C. P., Lithgow-Bertelloni, C., Jan. 2007. Faster seafloor spreading and lithosphere production during the mid-Cenozoic. Geology 35, 29.

DeMets, C., Gordon, R. G., Argus, D. F., Stein, S., 1994. Effect of recent revisions to the geomagnetic reversal time scale on estimates of current plate motions. Geophysical Research Letters 21, 2191–2194.

Di Giuseppe, E., Faccenna, C. E., Funiciello, F., van Hunen, J., Giardini, D., 2009. On the relation between trench migration, seafloor age, and the strength of the subducting lithosphere. Lithosphere 1.

England, P., McKenzie, D., 1982. A thin viscous sheet model for continental deformation. Geophys. J. Royal Astron. Soc. 70 (2), 295–321.

Funiciello, F., Faccenna, C., Giardini, D., Regenauer-Leib, K., 2003. Dynamics of retreating slabs: 2. insights from three-dimensional laboratory experiments. Journal of Geophysical Research 108.

Funiciello, F., Faccenna, C., Heuret, A., Lallemand, S., di Giuseppe, E., Becker, T. W., Jul. 2008. Trench migration, net rotation and slab mantle coupling. Earth and Planetary Science Letters 271, 233–240.

Garfunkel, Z., Anderson, C. A., Schubert, G., Jun. 1986. Mantle circulation and the lateral migration of subducted slabs. Journal of Geophysical Research 91, 7205–7223.

Gérault, M., Becker, T., Kaus, B., Moresi, L., Faccenna, C., Husson, L., 2012. The role of slabs and oceanic plate geometry for the net rotation of the lithosphere, trench motions, and slab return flow. Geochemistry, Geophysics, Geosystems.

Gerya, T., Dec. 2011. Future directions in subduction modeling. Journal of Geodynamics 52, 344–378.

Goes, S., Capitanio, F. A., Morra, G., Seton, M., Giardini, D., 2011. Signatures of downgoing plate-buoyancy driven subduction in cenozoic plate motions. Physics of the Earth and Planetary Interiors 184 (1-2), 1–13.

13

Gordon, R. G., Jurdy, D. M., Nov. 1986. Cenozoic global plate motions. Journal of Geophysical Letters 91, 12389–12406.

430 Gripp, A., Gordon, R., 2002. Young tracks of hotspots and current plate velocities young tracks of hotspots and current plate velocities. Geophysical Journal International 150, 321–361.

Heuret, A., Lallemand, S., Mar. 2005. Plate motions, slab dynamics and back-arc deformation. Physics of the Earth and Planetary Interiors 149, 31–51.

Husson, L., Conrad, C., Faccenna, C., 2011. Plate motions, Andean orogeny, and volcanism above the South Atlantic convection

435 cell. Earth and Planetary Science Letters.

Husson, L., Conrad, C. P., Faccenna, C., Jul. 2008. Tethyan closure, Andean orogeny, and westward drift of the Pacific Basin. Earth and Planetary Science Letters 271, 303–310.

Husson, L., Ricard, Y., 2004. Stress balance above subductions: application to the andes. Earth and Planetary Science Letters 222, 1037–1050.

440 Iaffaldano, G., Bunge, H.-P., Dixon, T. H., Oct. 2006. Feedback between mountain belt growth and plate convergence. Geology 34, 893.

Iaffaldano, G., Husson, L., Bunge, H.-P., Apr. 2011. Monsoon speeds up Indian plate motion. Earth and Planetary Science Letters 304, 503–510.

Jarrard, R., 1986. Relations among subduction parameters. Reviews of Geophysics 24, 217–284.

445 Karato, S.-i., Karki, B. B., 2001. Origin of lateral variation of seismic wave velocities and density in the deep mantle. Journal of Geophysical Research 106, 21771–21784.

Kincaid, C., Olson, P., Dec. 1987. An experimental study of subduction and slab migration. Journal of Geophysical Research 92, 13832–13840.

Kreemer, C., Holt, W. E., Haines, A. J., Jul. 2003. An integrated global model of present-day plate motions and plate boundary

450 deformation. Geophysical Journal International 154, 8–34.

Lallemand, S., Heuret, A., Boutelier, D., Sep. 2005. On the relationships between slab dip, back-arc stress, upper plate absolute motion, and crustal nature in subduction zones. Geochemistry, Geophysics, Geosystems 60, 9006.

Lallemand, S., Heuret, A., Faccenna, C., Funiciello, F., Jun. 2008. Subduction dynamics as revealed by trench migration. Tectonics 27, 3014.

455 Lambeck, K., Chappell, J., Apr 2001. Sea level change through the last glacial cycle. Science 292 (5517), 679–686.

Martinod, J., Husson, L., Roperch, P., Guillaume, B., Espurt, N., Nov. 2010. Horizontal subduction zones, convergence velocity and the building of the Andes. Earth and Planetary Science Letters 299, 299–309.

Mitrovica, J. X., Forte, A. M., Aug 2004. A new inference of mantle viscosity based upon joint inversion of convection and glacial isostatic adjustment data. Earth and Planetary Science Letters 225 (1-2), 177–189.

460 Nagel, T. J., Ryan, W. B. F., Malinverno, A., Buck, W. R., May 2008. Pacific trench motions controlled by the asymmetric plate configuration. Tectonics 27, 3005.

Parsons, B., Richter, F. M., Dec. 1980. A relation between the driving force and geoid anomaly associated with mid-ocean ridges. Earth and Planetary Science Letters 51, 445–450.

Ritsema, J., van Heijst, H. J., Woodhouse, J. H., Feb. 2004. Global transition zone tomography. Journal of Geophysical

465 Research (Solid Earth) 109, 2302.

Royden, L. H., Husson, L., 2006. Trench motion, slab geometry and viscous stresses in subduction systems. Geophysical Journal International 167 (2), 881–905.

Ruff, L., Kanamori, H., Oct. 1980. Seismicity and the subduction process. Physics of the Earth and Planetary Interiors 23, 240–252.

470 Schellart, W. P., Sep. 2008. Subduction zone trench migration: Slab driven or overriding-plate-driven? Physics of the Earth and Planetary Interiors 170, 73–88.

14

Stadler, G., Gurnis, M., Burstedde, C., Wilcox, L. C., Alisic, L., Ghattas, O., Aug. 2010. The Dynamics of Plate Tectonics and Mantle Flow: From Local to Global Scales. Science 329, 1033–.

Stegman, D. R., Freeman, J., Schellart, W. P., Moresi, L., May, D., Mar. 2006. Influence of trench width on subduction hinge retreat rates in 3-D models of slab rollback. Geochemistry, Geophysics, Geosystems 7, 3012.

Steinberger, B., Sutherland, R., O'Connell, R. J., Jul 2004. Prediction of emperor-hawaii seamount locations from a revised model of global plate motion and mantle flow. Nature 430 (6996), 167–173.

Tan, E., Choi, E., Thoutireddy, P., Gurnis, M., Aivazis, M., Jun. 2006. GeoFramework: Coupling multiple models of mantle convection within a computational framework. Geochemistry, Geophysics, Geosystems 7, 6001.

Turcotte, D., Schubert, G., 1982. Geodynamics. Journal of Geophysical Research.

Uyeda, S., Kanamori, H., 1979. Back-arc opening and the mode of subduction. Journal of Geophysical Research 84, 2017–2037.

Van Summeren, J., Conrad, C., Lithgow-Bertelloni, C., 2012. The importance of slab pull and a global asthenosphere to plate motions. Geochemistry, Geophysics, Geosystems.

Yamato, P., Husson, L., Braun, J., Loiselet, C., Thieulot, C., Apr. 2009. Influence of surrounding plates on 3D subduction dynamics. Geophysical Research Letters 36, 7303.

Zhong, S., Zuber, M. T., Moresi, L., Gurnis, M., 2000. Role of temperature-dependent viscosity and surface plates in spherical shell models of mantle convection. Journal of Geophysical Research 105, 11063–11082.
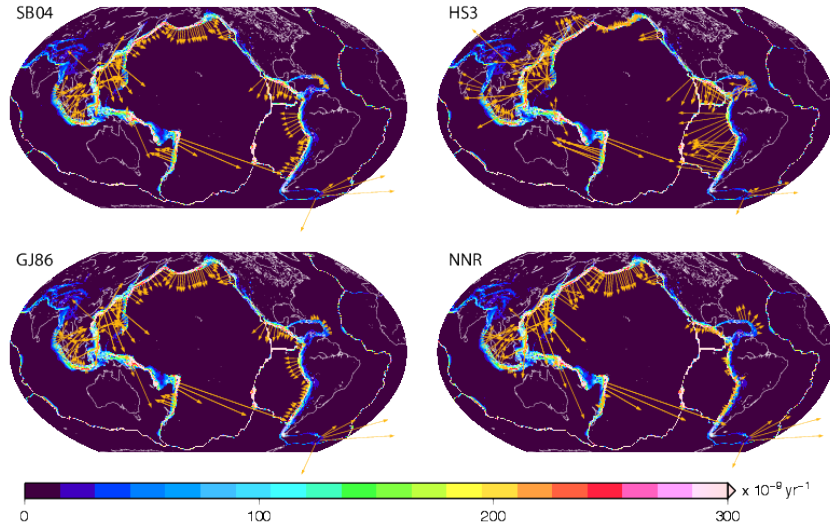
15

Figure 1: Normal component of trench migration rates (orange vectors, from Funiciello et al., 2008) in the reference frames *SB04* (Steinberger et al., 2004), *HS3* (Gripp and Gordon, 2002), *GJ86* (Gordon and Jurdy, 1986), *NNR* (DeMets et al., 1994). World Strain Map on the background (second invariant of strain rate, Kreemer et al., 2003).
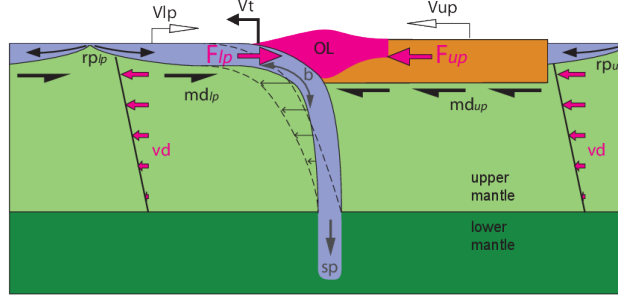
Supplementary information

Figure 2: Forces balance around subduction zones. V_t, V_{lp} and V_{up} are the trench, lower plate and upper plate velocities, respectively. F_{lp} and F_{up} are the total forces exerted by the upper and lower plates onto the plate interface. md is the sublithospheric mantle drag; OL is the orogenic load, vd is the viscous dissipation due to the rollback component of subduction, in the poloidal field. sp, b, and rp are the slab pull, bending force, and ridge push. Subscripts $_{lp}$ and $_{up}$ refer to the lower and upper plates.
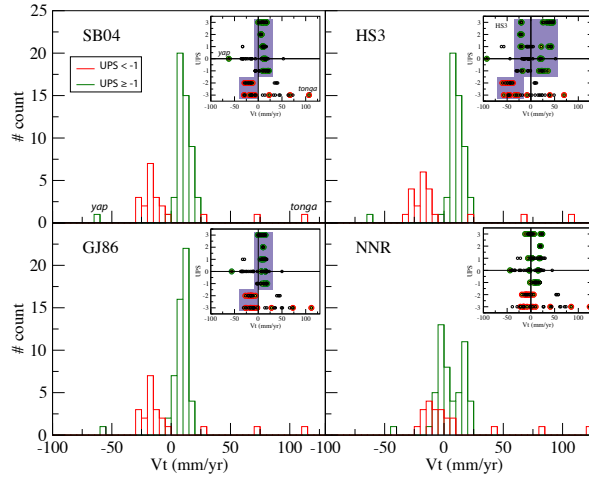
Figure 3: Distribution of trench velocities for upper plates undergoing compression (green, $UPS > -1$) and upper plates undergoing extension (red, $UPS < -1$) for circum-Pacific trenches, in the reference frames $SB04$ (Steinberger et al., 2004), $HS3$ (Gripp and Gordon, 2002), $GJ86$ (Gordon and Jurdy, 1986), NNR (DeMets et al., 1994). Insets show upper plate strain UPS as a function of trench velocity Vt for all trenches (black dots), and circum-Pacific only (red and green circles). Purple domains encompass more than 95% circum-Pacific data. The threshold $UPS{\sim}\text{-}1$ isolates the red and black histograms.
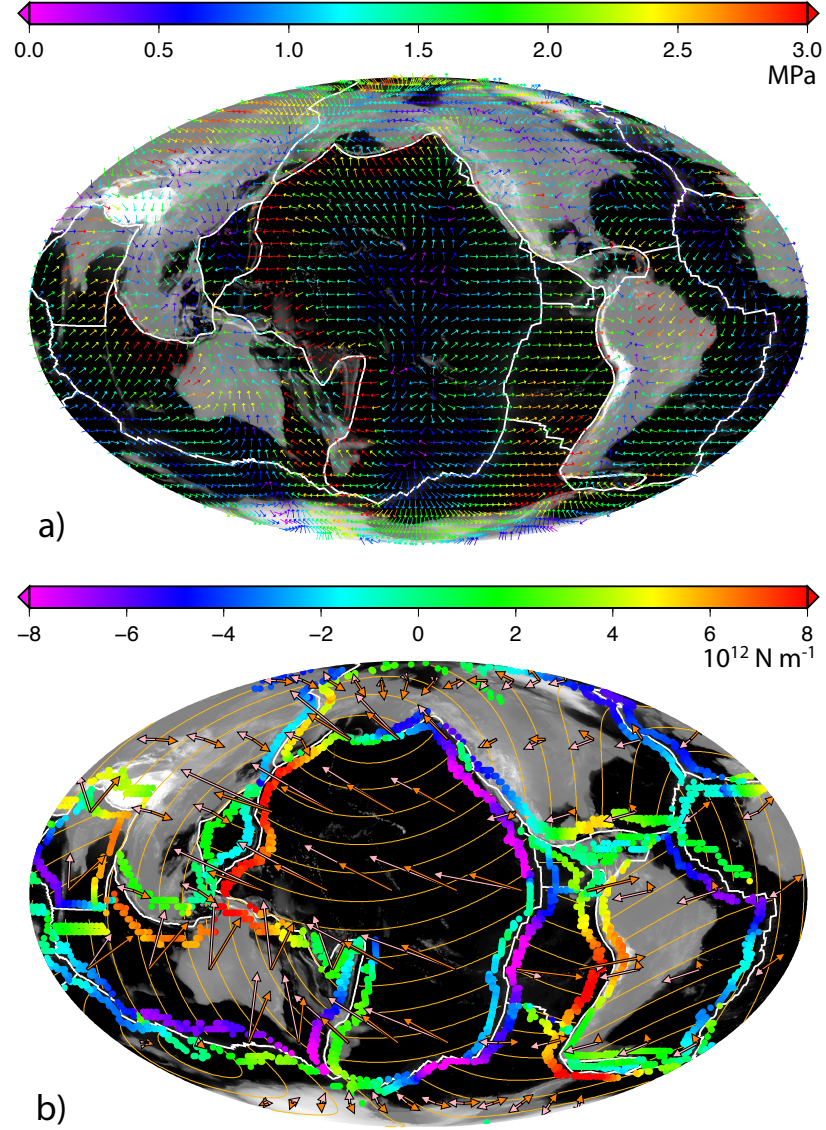
17

Figure 4: a) Shear stresses underneath the lithosphere due to mantle drag from the convecting mantle excited by internal loads (after Conrad and Behn, 2010, see text). b) Colored dots show the normal component of plate boundary forces (per unit length) due to mantle drag underneath the lithosphere (from panel a), integrated along the orange small circles, whose Euler poles are defined for each plate by the net torque exerted by mantle drag. The value at one end of a small circle is the opposite of its other end counterpart. Orange and light pink arrows show plate motion in the end members NNR (DeMets et al., 1994) and HS3 (Gripp and Gordon, 2002) reference frames, respectively.
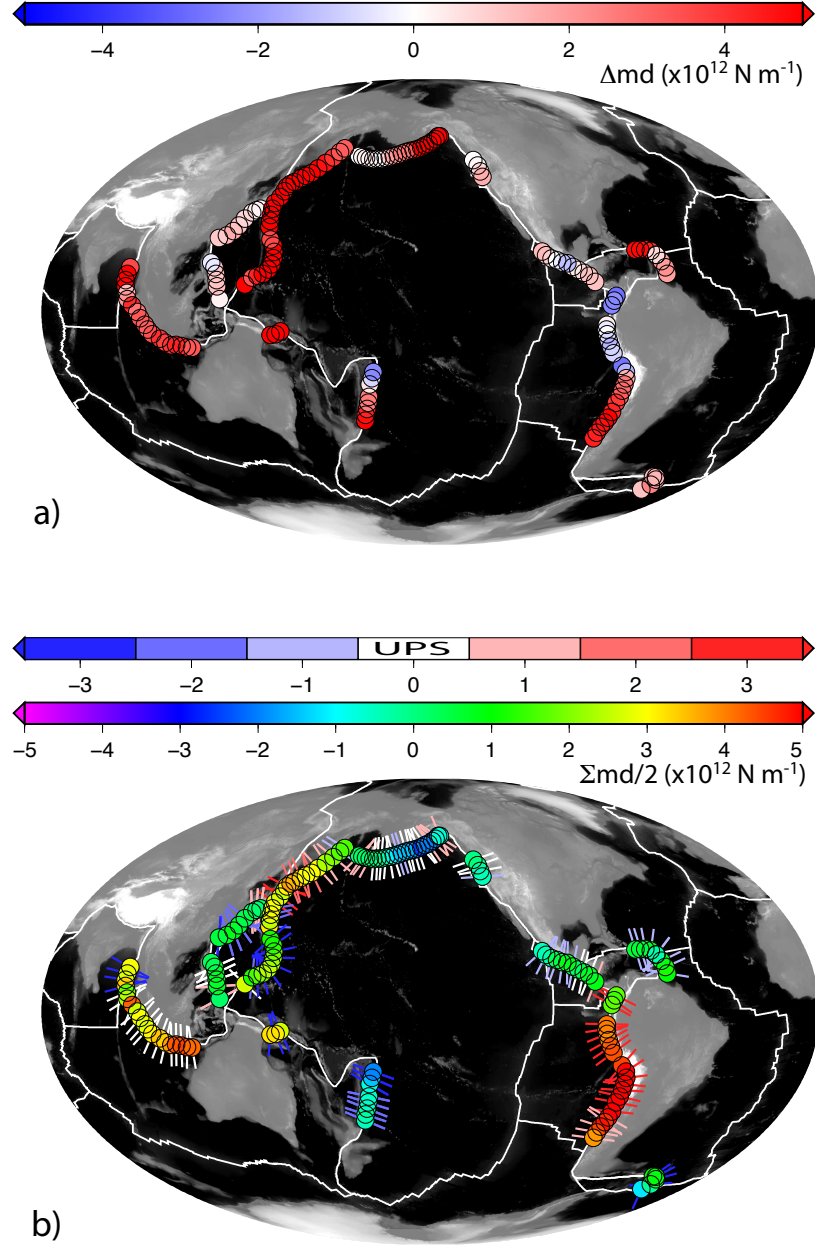
Figure 5: a) Δmd (colored dots), the difference between integrated mantle drag from the upper and lower plates (per unit trench length, see Fig. 4b), together with trench velocities V_t (arrows) in the reference frame $SB04$ (Steinberger et al., 2004), that spins at an intermediate rate between the end members NNR and $HS3$, see Fig. 1b). $\Sigma md/2$ (colored dots), the mean of integrated mantle drags from both the upper and lower plates (see Fig. 4b), together with upper plate strain indicators UPS (from Heuret and Lallemand, 2005, colored bars).

19
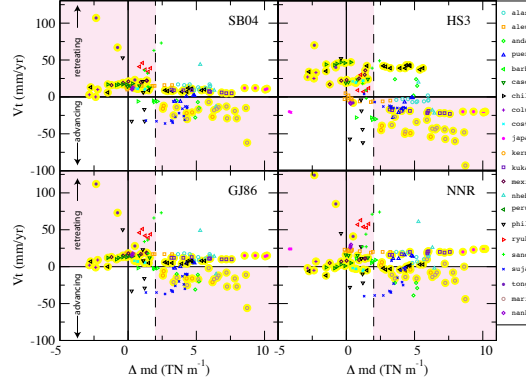
Figure 6: Normal component of trench motion V_t as a function of $\Delta md = md_{lp} - md_{up}$, the trench normal component of the integrated mantle drag from both the upper and lower plates (counted positive trenchward). Yellow dots refer to circum-Pacific trenches (excluding Alaska and Aleutians, see text). Trenches names are abbreviated as follow: *alas*ka; *aleut*ian; *anda*man; *puer*to-rico; *barb*ados; *casc*adia; *chil*e; *colu*mbia; *cost*a-rica; *japa*n; *kerm*adec; *kuka*, kuril-kamtchatka; *mexi*co; *nheb*, new hebrides; *peru*; *phil*ipines; *ryu*kyu; *sand*wich; *suja*, sumatra-java; *tong*a; *mari*ana; *nank*ai.
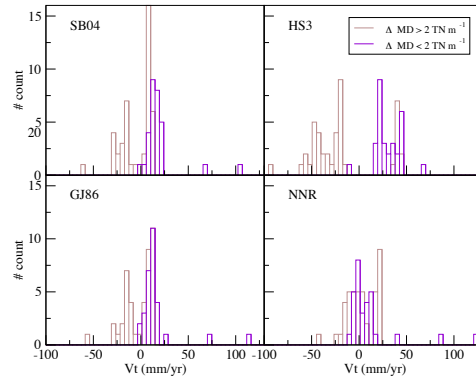
Figure 7: Distribution histograms of V_t for $\Delta md > 2\,TN\,m^{-1}$ (brown) and for $\Delta md < 2\,TN\,m^{-1}$ (purple) for circum-Pacific trenches only (yellow dots, fig. 6).
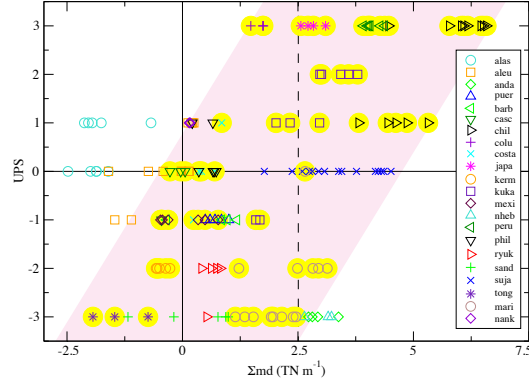
20

Figure 8: Upper plate strain UPS as a function of $\Sigma md/2 = (md_{lp} + md_{up})/2$, the mean trench normal integrated mantle drag force from both the upper and lower plates (counted positive trenchward). Yellow dots refer to circum-Pacific trenches (yellow dots, fig. 6). See trench names fig. 6
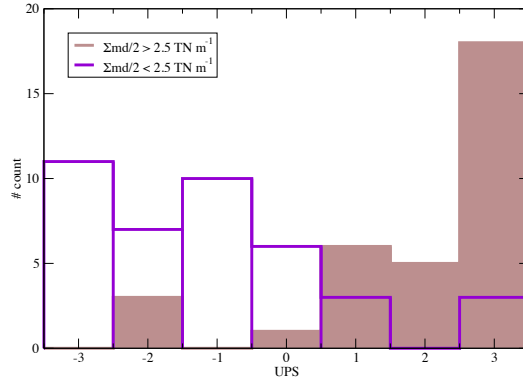

Figure 9: Distribution histograms of UPS for $\Sigma md/2 > 2.5 \times 10^{12}$ N m^{-1} (brown) and for $\Sigma md/2 < 2.5 \times 10^{12}$ N m^{-1} (purple) for circum-Pacific trenches only (yellow dots, fig. 8).
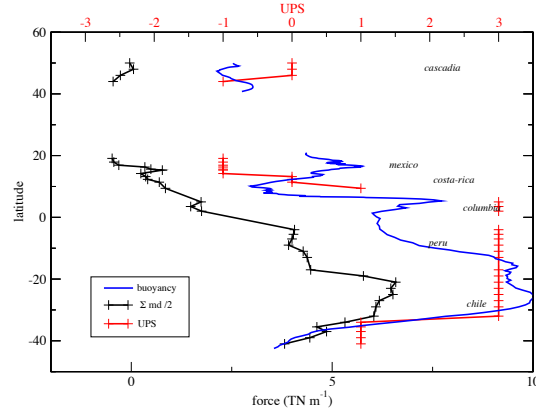
Figure 10: $\Sigma md/2$ (solid black, the mean trench normal integrated mantle drag force from both the upper and lower plates), upper plate strain (red) and orogenic buoyancy force (dashed, black, see Husson and Ricard, 2004) as a function of latitude, for West (a) and East Pacific trenches (b). Symbols + are data points from Heuret and Lallemand (2005).
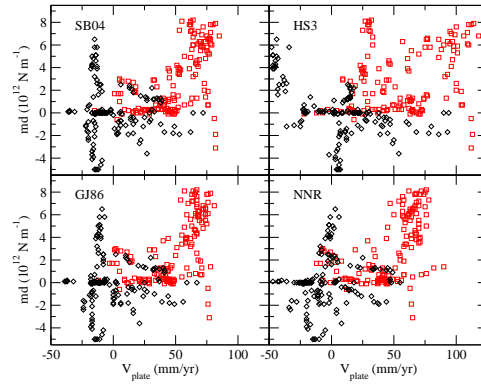

Figure 11: Supplementary figure 1: Integrated mantle drag force per unit trench length as a function of upper (black) and lower (red) plate motion in the reference frames *SB04* (Steinberger et al., 2004), *HS3* (Gripp and Gordon, 2002), *GJ86* (Gordon and Jurdy, 1986), *NNR* (DeMets et al., 1994).